ORIGINAL RESEARCH

Role of Spdef in the Regulation of Muc5b Expression in the Airways of Naive and Mucoobstructed Mice

Gang Chen, Allison S. Volmer, Kristen J. Wilkinson, Yangmei Deng, Lisa C. Jones, Dongfang Yu, Ximena M. Bustamante-Marin, Kimberlie A. Burns, Barbara R. Grubb, Wanda K. O'Neal, Alessandra Livraghi-Butrico, and Richard C. Boucher

Marsico Lung Institute and University of North Carolina Cystic Fibrosis Center, University of North Carolina at Chapel Hill, Chapel Hill, North Carolina

Abstract

Understanding how expression of airway secretory mucins MUC5B and MUC5AC is regulated in health and disease is important to elucidating the pathogenesis of mucoobstructive respiratory diseases. The transcription factor SPDEF (sterile α-motif pointed domain epithelial specific transcription factor) is a key regulator of MUC5AC, but its role in regulating MUC5B in health and in mucoobstructive lung diseases is unknown. Characterization of *Spdef*-deficient mice upper and lower airways demonstrated region-specific, *Spdef*-dependent regulation of basal Muc5b expression. Neonatal *Spdef*-deficient mice exhibited reductions in BAL Muc5ac and Muc5b. Adult *Spdef*-deficient mice partially phenocopied *Muc5b*-deficient mice as they exhibited reduced Muc5b in nasopharyngeal and airway epithelia but not in olfactory Bowman glands, 75% incidence of nasopharyngeal hair/mucus plugs, and mild bacterial otitis media, without defective mucociliary clearance in the nasopharynx. In contrast, tracheal mucociliary clearance was reduced in *Spdef*-deficient mice in the absence of lung disease. To evaluate the role of *Spdef* in the development and persistence of Muc5b-predominant mucoobstructive lung disease, *Spdef*-deficient mice were crossed with *Scnn1b*-transgenic (*Scnn1b*-Tg) mice, which exhibit airway surface dehydration-induced airway mucus obstruction and inflammation. *Spdef*-deficient *Scnn1b*-Tg mice exhibited reduced Muc5ac, but not Muc5b, expression and BAL content. Airway mucus obstruction was not decreased in *Spdef*-deficient *Scnn1b*-Tg mice, consistent with Muc5b-dominant *Scnn1b* disease, but increased airway neutrophilia was observed compared with *Spdef*-sufficient *Scnn1b*-Tg mice. Collectively, these results indicate that *Spdef* regulates baseline Muc5b expression in respiratory epithelia but does not contribute to Muc5b regulation in a mouse model of Muc5b-predominant mucus obstruction caused by airway dehydration.

Keywords: *Spdef*; *Scnn1b*-Tg; mucoobstructive lung disease; mucociliary clearance

Clinical Relevance

In our present study, we identified the role of SPDEF (sterile α-motif pointed domain epithelial specific transcription factor) in the regulation of mucin production in the upper and lower airways of the mouse. We raise caution that targeting SPDEF may not be effective in treating mucus obstruction caused by airway surface dehydration such as that seen in cystic fibrosis.

Mucoobstructive lung diseases, such as the chronic bronchitic component of chronic obstructive pulmonary disease (COPD), cystic fibrosis, and asthma, share alterations in mucus biology as a component of their pathophysiology (1–3). These diseases are associated with dysregulated mRNA expression, protein expression, secretion, and extracellular concentration of the two major airway-secreted mucins, MUC5AC and MUC5B. Classically, the paradigm for the human respiratory tract has held that

MUC5B is expressed primarily in the mucous cells of submucosal glands (4), and MUC5AC is secreted from the superficial airway goblet cells (5, 6). However, recent data describe Muc5b expression in airway superficial epithelia during health and that Muc5b is essential for normal mucociliary clearance (MCC) and innate immune functions (7–11). Although MUC5AC is not the predominant secreted airway mucin during health, it can be robustly upregulated by a wide variety of stimuli, including developmental cues (8), microbial and growth factors, and inflammatory cytokines (12). Studies elucidating the molecular signals that regulate goblet cell differentiation are ongoing (reviewed in reference 13), but a comprehensive understanding of how these processes are regulated during health versus disease is lacking.

One gene recently described as a key transcriptional regulator of mucin expression is *SPDEF/Spdef*. SPDEF was originally classified as a prostate epithelium–specific Ets transcription factor (14), but it has since been recognized as integral to goblet cell differentiation in the intestine, lung, and conjunctiva (15–19). Recent work has demonstrated that *Spdef* is involved in T-helper cell type 2 (Th2)-driven goblet cell differentiation during postnatal lung development in mice (20). Spdef is similarly required for Th2 inflammation–driven goblet cell metaplasia and increased Muc5ac secretion in response to ovalbumin and house dust mite challenge, acting through the IL-13/IL-4 receptor-α and the STAT6 (signal transducer and activator of transcription 6) axis (21, 22). Furthermore, *Spdef* overexpression induces a number of genes regulating mucin biosynthesis/glycosylation and goblet cell differentiation and suppresses genes involved in airway epithelial Na$^+$ and fluid absorption (e.g., *Scnn1b* and *Scnn1 g*) (17). In addition to its role as a transcription factor, Spdef also has cytoplasmic functions regulating innate immunity because its overexpression blunts LPS-driven neutrophilia *in vivo* and inhibits MyD88 (myeloid differentiation primary response 88)-mediated cytokine production and Toll/IL-1 receptor domain-containing adapter-inducing IFN-mediated IFN-β production upon rhinovirus challenge *in vitro* (23).

Although Spdef regulation of Muc5ac expression in the respiratory tract in response to Th2 challenge has been amply

documented, its influence on Muc5b, in both health and disease, has not been described. To elucidate the role of SPDEF in health, *Spdef*-deficient mice were characterized with respect to regulation of airway Muc5b and Muc5ac expression, MCC, and respiratory tract pathology. In the context of disease, the airway-targeted overexpression of the β-subunit of the epithelial sodium channel (β-ENaC, encoded by the *Scnn1b* gene) produces accelerated Na$^+$ absorption and airway surface liquid (ASL) volume depletion. ASL volume depletion in turn produces the mucus hyperconcentration/stasis and chronic inflammation (24–31) that recapitulate the pathologic features of human mucoobstructive diseases associated with an increase in MUC5B, including cystic fibrosis, chronic bronchitis, and COPD (31–35). Therefore, to investigate the role of Spdef in a complex disease model dominated by Muc5b-enriched mucus hyperconcentration and accumulation, *Spdef*-deficient mice were crossed with *Scnn1b*-Tg mice and their progeny phenotyped for severity of lung disease using measures of airway mucus obstruction and inflammation.

Methods

Mice
Mice were maintained and studied under protocols approved by the University of North Carolina Institutional Animal Care and Use Committee. Mice were housed in individually ventilated microisolator cages in a specific pathogen-free facility at the University of North Carolina at Chapel Hill on a 12-hour/12-hour day/night cycle. Mice were fed regular chow and given water *ad libitum*. F10 C57BL/6N *Spdef*$^{-/-}$ mice were obtained from Dr. Jeffrey Whitsett's laboratory (Cincinnati Children's Hospital Medical Center). *Spdef*$^{+/-}$ mice were bred with congenic C57BL/6N *Scnn1b*-Tg mice (25) to generate *Spdef*-deficient *Scnn1b*-Tg mice. Before Postnatal Day (PND) 5, pups were toe clipped for identification and genotyping as previously described (20, 24). Mice studied were littermates when possible, age matched, and of both sexes.

Mouse Phenotyping and Histology
Mouse lungs were immersion fixed in 10% neutral-buffered formalin, embedded, and sectioned at 5-μm thickness. Mouse heads

were fixed in 10% NBF, decaled 24 hrs in Formical-4, and the nasal cavity was cut at the level of the upper incisors, in front of the incisive papilla, at the level of the second palatal ridge, and at the level of the third molar (36) to yield four sequential levels. Hematoxylin and eosin staining was performed using Richard-Allan Scientific hematoxylin and eosin (catalogue numbers 7221 and 7111). The protocol for Alcian blue/periodic acid–Schiff (AB-PAS) staining involved 10 minutes in AB, pH 2.5 (catalogue number 867; Anatech) to highlight acidic proteoglycans (teal), a 10-minute wash in running tap water, 5 minutes in 0.5% periodic acid, a rinse in tap water, 15 minutes in Schiff's reagent (catalog number SS32-500; Fisher Scientific) to highlight neutral proteoglycans (magenta), 20 dips in sulfurous rinse, and a 10-minute wash in running tap water. With this method, airway mucus typically exhibits a combination of magenta and teal color (gradation of purple/blue) stain. Experimental groups were processed using the same batch of fixative and staining reagents.

Immunohistochemistry and Western Blot Analysis
Muc5ac and Muc5b immunohistochemical staining was performed as previously described (17). Briefly, after antigen retrieval with citrate buffer and heat, MUC5AC (ab3649; Abcam), MUC5B antibodies (SC20119; Santa Cruz Biotechnology), FOXA3 antibody (SC5361; Santa Cruz Biotechnology), and acetylated α-tubulin antibody (T7451; Sigma-Aldrich) were used for immunostaining. Morphometric analysis of volume density (V$_S$) for AB-PAS$^+$, Muc5ac$^+$, or Muc5b$^+$ staining was performed as previously described (26, 37) on cross-sections of the left lobe main stem bronchus serially cut every 2 mm starting at the hilum to yield systematic sampling of the proximal, intermediate, and distal airways. The histological micrographs shown in the figures are montages acquired using the Olympus VS120 Virtual Slide Scanning System (Olympus). Slides were scanned at 40× magnification unless otherwise specified. Quantification of secreted mucins in BAL by Western blotting was performed as previously described (26).

MCC Assay

MCC was measured in the upper (anterior nasopharynx) and lower (trachea) airways as previously described (38), using fluorescent microbead tracking and quantification in KOH-solubilized lungs, respectively.

Airway Bioelectric Studies

Adult mice were studied at 4–5 months of age. All studies were performed blinded with respect to genotype. Details of the Ussing chamber preparations have been published previously (39). Amiloride (10^{-4} M apical addition) was used to block electrogenic Na^+ absorption. Forskolin (10^{-5} M apical) and UTP (10^{-4} M apical) were used to induce anion secretion via an increase in intracellular cAMP and intracellular Ca^{2+} concentrations, respectively. All drugs were purchased from Sigma-Aldrich with the exception of UTP (Amersham Pharmacia Biotech).

Middle Ear Lavage for Assessment of Otitis Media

Middle ear lavage was performed as previously described (7) by instilling and retrieving sterile PBS in the tympanic bulla and plating serial dilutions of the retrieved fluid on BD Columbia anaerobe sheep blood agar (Becton Dickinson). Colony-forming units were enumerated after 24-hour growth at 37°C in a candle jar (microanaerobiosis).

Mouse Tracheal Epithelial Cell Culture and Ciliary Beat Frequency Assays

Mouse tracheal epithelial cell (mTEC) isolation and culturing were carried out according to protocols previously described (40) using PluriQ differentiation media (Stem Cell, Inc.), Millicell inserts (PICM01250; MilliporeSigma), and culturing for 4 weeks at the air–liquid interface to allow full differentiation. Ciliary beat frequency (CBF) was measured in fully hydrated conditions according to previously described protocols (38, 41).

RNA Analysis

Cellular RNA was isolated with TRIzol reagent and the Direct-zol RNA Miniprep Kit (Zymo Research). Total RNAs (500 ng) were reverse transcribed to cDNA by using the Verso cDNA Synthesis Kit (Thermo Fisher Scientific). Quantitative RT-PCR was performed using TaqMan probes and primer sets (Thermo Fisher Scientific) specific for *Spdef* (Mm00600221_m1), Muc5ac (Mm01276718_m1), Muc5b (Mm00466391_m1), Scnn1a (Mm00803386_m1), *Scnn1b* (Mm00441215_m1), and Scnn1g (Mm00441228_m1). A probe and primer set for Gapdh (Mm99999915_g1) was used as a normalization control because its expression did not significantly change among groups. PCRs were performed using the Applied Biosystems QuantStudio 6 PCR System (Thermo Fisher Scientific).

Statistics

Student's *t* test (two tailed, unpaired) (Prism 6 software; GraphPad Software) was used for comparison of statistical differences between two groups. One-way ANOVA followed by Dunnett's multiple-comparisons test (Prism 6) was used to compare three or more groups. *P* values less than 0.05 were considered significantly different. Data are presented as mean ± SD unless otherwise indicated in the figure legends.

Results

Characterization of Naive Upper Airways Reveals Region-Specific, Spdef-Dependent Regulation of Basal Muc5b Expression

Because Spdef could influence both the level of expression and the glycosylation of airway mucins, we first evaluated the upper airways (nasal cavities and nasopharynx) of adult (PND 48) *Spdef*-deficient (*Spdef*$^{-/-}$) versus wild-type (WT; *Spdef*$^{+/+}$) mice for glycoconjugates by using the AB-PAS histochemical stain and for Muc5b by using immunohistochemistry. *Spdef* deficiency produced a striking reduction in both AB-PAS and Muc5b-positive staining of the surface airway epithelium of the nasal septum, vomeronasal organ, and anterior nasopharynx, but not in the Bowman glands underlying the olfactory epithelium, as compared with WT mice (Figures 1A and 1B). Of note, currently available antibodies specific for murine Muc5ac do not work in decalcified specimens, which prevented Muc5ac evaluation in the upper airways of *Spdef*$^{-/-}$ mice versus WT littermates.

During the course of these studies, we noticed that a high proportion (11 out of 16) of adult (PNDs 43–170) *Spdef*$^{-/-}$ mice exhibited visible "hair/mucus" plugs in the nasopharyngeal cavity (Figure 1C), which resembled those found in *Muc5b*-knockout (*Muc5b*$^{-/-}$) mice (7). *Spdef*$^{-/-}$ mice also exhibited bacterial otitis media, though milder than *Muc5b*$^{-/-}$ mice (Figure 1D). Unlike adult (>3-month-old) *Muc5b*$^{-/-}$ mice, *Spdef*$^{-/-}$ mice did not have reduced MCC in the anterior nasopharynx (Figure 1E) as compared with WT littermates. No weight loss or reduction in survival was noted in *Spdef*$^{-/-}$ mice (not shown).

Analysis of tracheal submucosal glands in PND 42 mice revealed that loss of Spdef inhibited mucous cell differentiation (Figure 2A) as previously reported (17) and decreased AB$^+$ staining, whereas PAS staining was preserved (Figure 2B). Muc5b immunostaining was reduced in *Spdef*$^{-/-}$ submucosal glands (Figure 2C) and in tracheal surface epithelium (Figure 2D), whereas Muc5ac expression was absent in submucosal gland and tracheal surface epithelium of both *Spdef*$^{-/-}$ mice and WT littermates (Figure 2E).

Spdef Deficiency in Naive Mouse Lower Airways Causes Defective Muc5b and Muc5ac Expression, Decreased MCC, and Altered Airway Epithelial Ion Transport

Extending our analysis to the lower airways, we first considered the effect of *Spdef* deficiency during the early postnatal period, which in mouse airways is normally characterized by a transient increase in AB-PAS–positive cells (24). Qualitatively, airway epithelial cells from the main stem bronchi of PND 7–10 WT mice exhibited a mixture of magenta and blue AB-PAS staining, indicating the presence of both neutral and acidic glycoconjugates, respectively. In contrast, bronchi from *Spdef*-deficient littermates exhibited reduced and less acidic (i.e., less blue/purple) AB-PAS staining (Figure 3A). These changes were associated with a reduction in both Muc5ac and Muc5b protein levels in unfractionated BAL samples collected at the same age (Figure 3B and Figure E1A in the data supplement).

Similar qualitative changes in AB-PAS–positive staining were also observed in the lower airways (i.e., intrapulmonary main stem bronchi) of adult (PND 42) *Spdef*-deficient mice as compared with WT
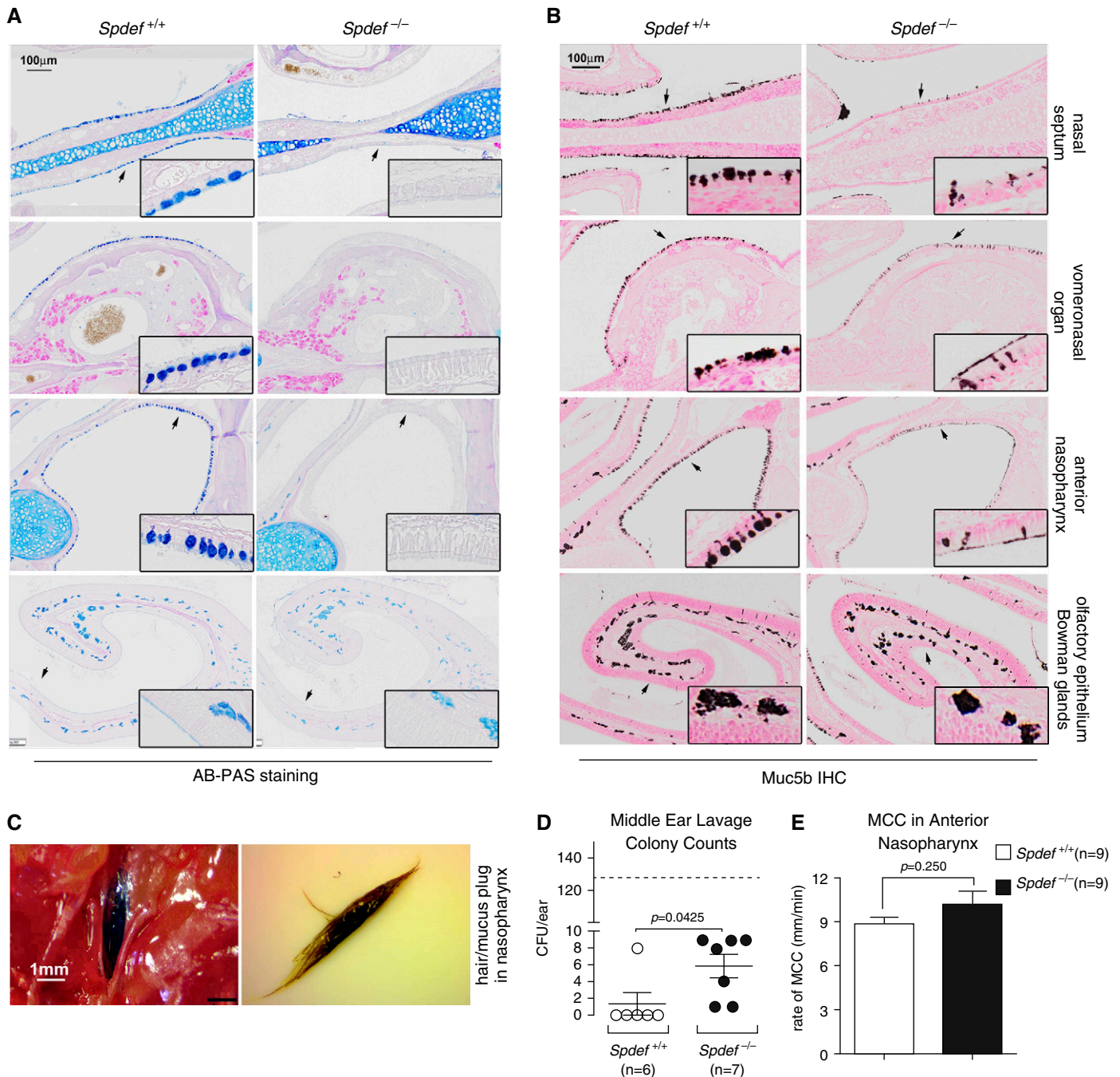
Figure 1. Mucin-related phenotypes in the upper airways of adult Spdef (sterile α-motif pointed domain epithelial specific transcription factor)-deficient mice. (*A* and *B*) Representative micrographs illustrating (*A*) Alcian blue/periodic acid–Schiff (AB-PAS) stain and (*B*) Muc5b immunohistochemical (IHC) stain of various upper airway tissues (indicated on the right-hand side), comparing staining patterns between *Spdef*-sufficient (*Spdef*^{+/+}) and *Spdef*-deficient (*Spdef*^{−/−}) naive mice at Postnatal Day (PND) 56. Insets show high-magnification views of areas highlighted by the arrows in the low-magnification panels. Micrographs are representative of at least three mice for each genotype, and they are montages acquired with a slide scanner, as described in the METHODS section of the text. Scale bars: 100 μm. (*C*) Representative image of a nasopharyngeal hair/mucus plug *in situ* (left panel) or removed (right panel) from a 5.6-month-old *Spdef*^{−/−} mouse. Scale bar: 1 mm. (*D*) Culturable bacteria counts in middle ear lavage from *Spdef*^{−/−} (solid dots) and control (open dots) mice at 4–5 months of age (*n* = 6–7/genotype). Dashed line represents the average colony-forming units per ear for Muc5b-knockout mice, which exhibit highly penetrant bacterial otitis media with effusion (7). (*E*) Mucociliary clearance (MCC) measurements in the anterior nasopharynx of naive *Spdef*-sufficient (*Spdef*^{+/+}; open bar) and *Spdef*-deficient (*Spdef*^{−/−}; solid bar) mice (*n* = 9/genotype) at ages PND 43 (*n* = 7) and PND 170 (*n* = 2) for both genotypes.
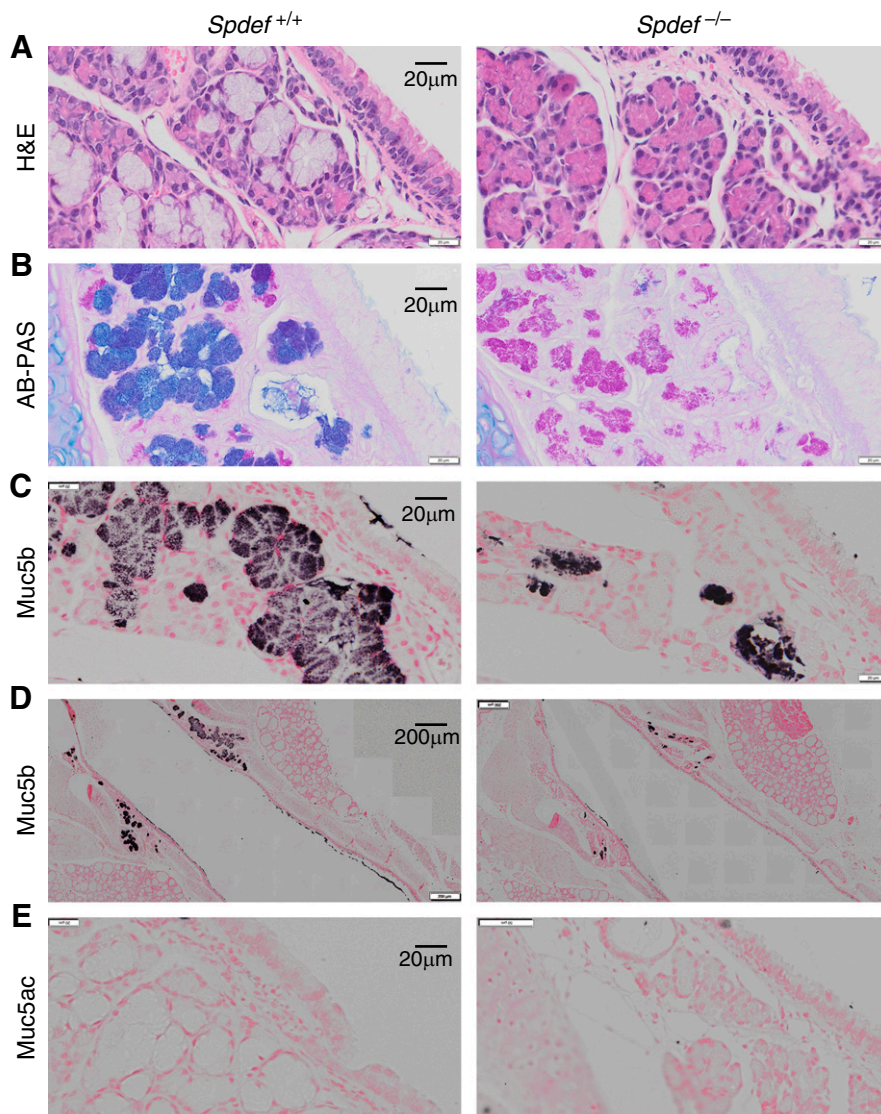
Figure 2. Spdef is required for mucous cell differentiation and Muc5b expression in tracheal submucosal gland and superficial epithelium. Representative micrographs illustrating mucous cell differentiation (*A*) hematoxylin and eosin (H&E) staining, (*B*) glycoconjugates (AB-PAS staining), (*C* and *D*) Muc5b (submucosal glands and superficial epithelium, respectively), and (*E*) Muc5ac immunohistochemistry in PND 42 $Spdef^{-/-}$ and wild-type littermates. Micrographs are montages acquired with a slide scanner as described in the METHODS section of the text. Scale bars: 20 μm (*A–C* and *E*) and 200 μm (*D*).

mice and WT littermates (Figure 3C, bottom panel; Figure 3F; and Figure E2B). Consistent with these observations, the levels of Muc5b in BAL were slightly reduced in adult $Spdef^{-/-}$ mice as compared with WT littermates, whereas Muc5ac was undetectable in both genotypes (Figure 3G). Notably, both *Muc5ac* and *Muc5b* mRNA expression was downregulated in whole lung from adult *Spdef*-deficient mice as compared with WT littermates (Figure 3H).

Unlike the observations in the upper airways, loss of *Spdef* was accompanied by a significant reduction in tracheal MCC in adult mice (Figure 3I). Reduced MCC has been associated with several mechanisms, including *1*) reduced Muc5b expression (7, 38), *2*) airway surface dehydration (26), or *3*) reduced ciliated cell numbers/function (41). Because *Spdef* is known to regulate several genes involved in the MCC system, we tested for mechanisms in addition to the observed reduction in Muc5b level that could produce low MCC in $Spdef^{-/-}$ mice. To test if loss of *Spdef* affected the bioelectrical properties of epithelial cells lining the mouse trachea, Ussing chamber analyses of freshly excised tracheas from WT and *Spdef*-deficient adult mice were performed. *Spdef* deficiency was associated with increased ENaC activity, as indexed by elevated basal and amiloride-sensitive short-circuit currents (I_{sc}) (Figure 3J). This alteration was accompanied by a small but significant increase in forskolin-stimulated anion secretion but no change in UTP responses. Because *Spdef* overexpression has been shown to inhibit transcription of the β- and γ-ENaC subunits (17), which are believed to be rate limiting for murine airway epithelial ENaC function (42), we tested whether loss of *Spdef* was associated with increased transcription of the α-, β-, or γ-ENaC subunits (*Scnn1a*, *Scnn1b*, *Scnn1g*). This analysis revealed a subtle but significant increase in whole-lung mRNA expression of the α-subunit, but not of the β- and γ-subunits, in $Spdef^{-/-}$ mice as compared with WT littermates (Figure E3A).

To investigate whether loss of *Spdef* altered ciliated cell populations and/or changed CBF, we quantified ciliated cell numbers in tracheas by morphometric analysis of acetylated α-tubulin staining (a ciliated cell-specific marker). There were no significant differences in acetylated α-tubulin$^+$ V_S or cell number in tracheas

littermates (Figure 3C, upper panel). To quantitate the AB-PAS–positive material present in the airways of $Spdef^{-/-}$ mice and WT littermates, morphometric analysis of AB-PAS–positive volume density (V_S), which does not discriminate between magenta and blue staining, was performed across three different levels of the left main stem bronchus (proximal = at the hilum, intermediate = 2 mm caudal to the hilum, and distal = 4 mm caudal to the hilum) (Figure E1B). These analyses indicated that

Spdef-deficient mice exhibited a trend toward reduced AB-PAS V_S in the proximal but not distal regions of the main stem bronchus (Figure 3D). Immunohistochemical localization of Muc5b and Muc5ac in serial sections followed by morphometry indicated that Muc5b staining mirrored the pattern observed for the AB-PAS staining (Figure 3C, middle panel; Figure 3E; and Figure E2A), whereas Muc5ac was undetectable at baseline in both $Spdef^{-/-}$
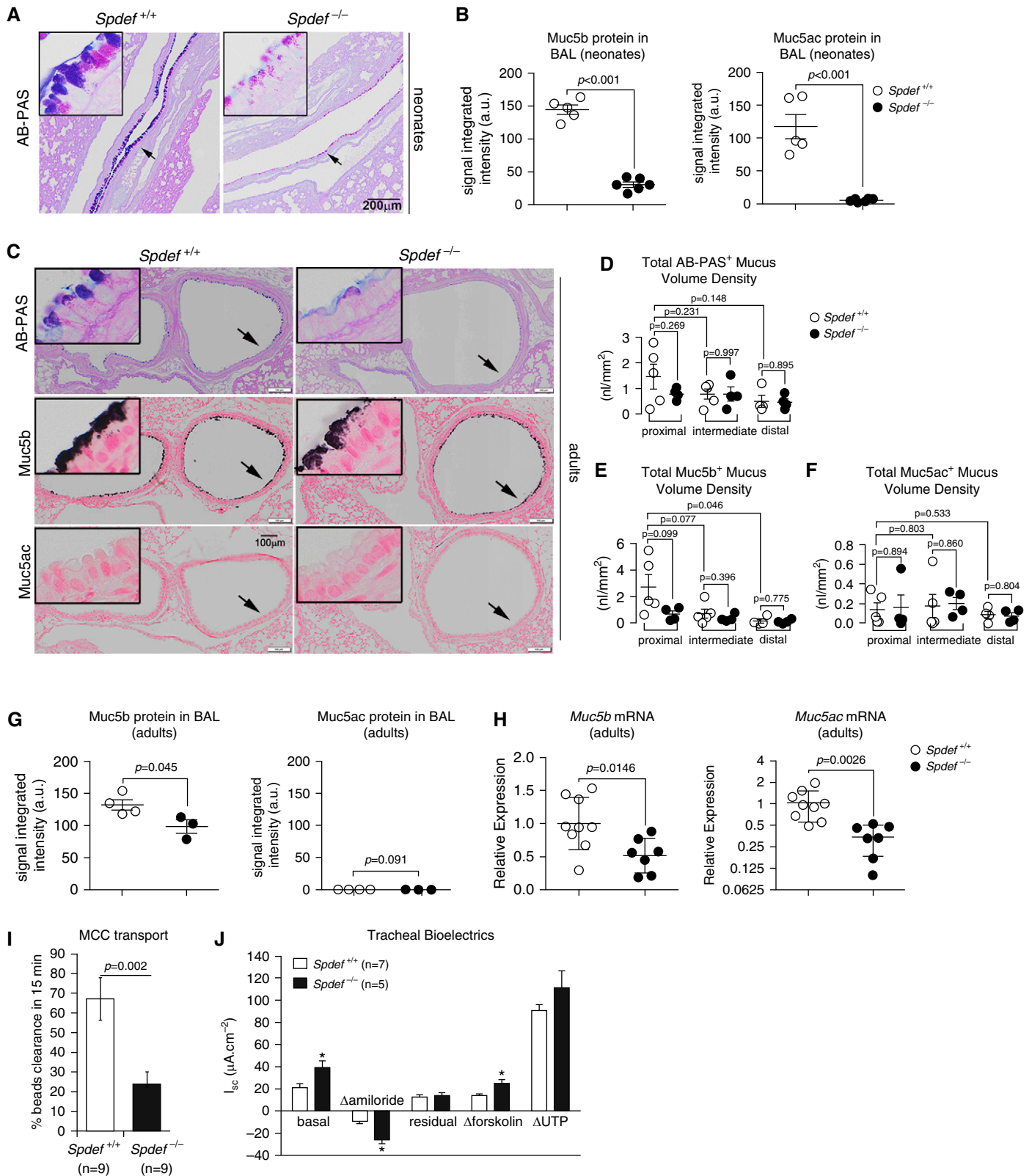
Figure 3. Mucin-related phenotypes in lower airways of Spdef-deficient neonatal and adult mice. (*A*) Representative micrographs illustrating AB-PAS staining in neonatal (PND 10) naïve Spdef-sufficient (*Spdef*$^{+/+}$) and Spdef-deficient (*Spdef*$^{-/-}$) mice. Insets show high-magnification views of areas highlighted by the arrows in the low-magnification panels. Micrographs are representative of at least three mice for each genotype. Scale bar: 200 μm. (*B*) Densitometric analysis of Muc5b- and Muc5ac-specific signaling in agarose Western blots of BAL from naïve *Spdef*$^{+/+}$ and *Spdef*$^{-/-}$ mice at PND 10
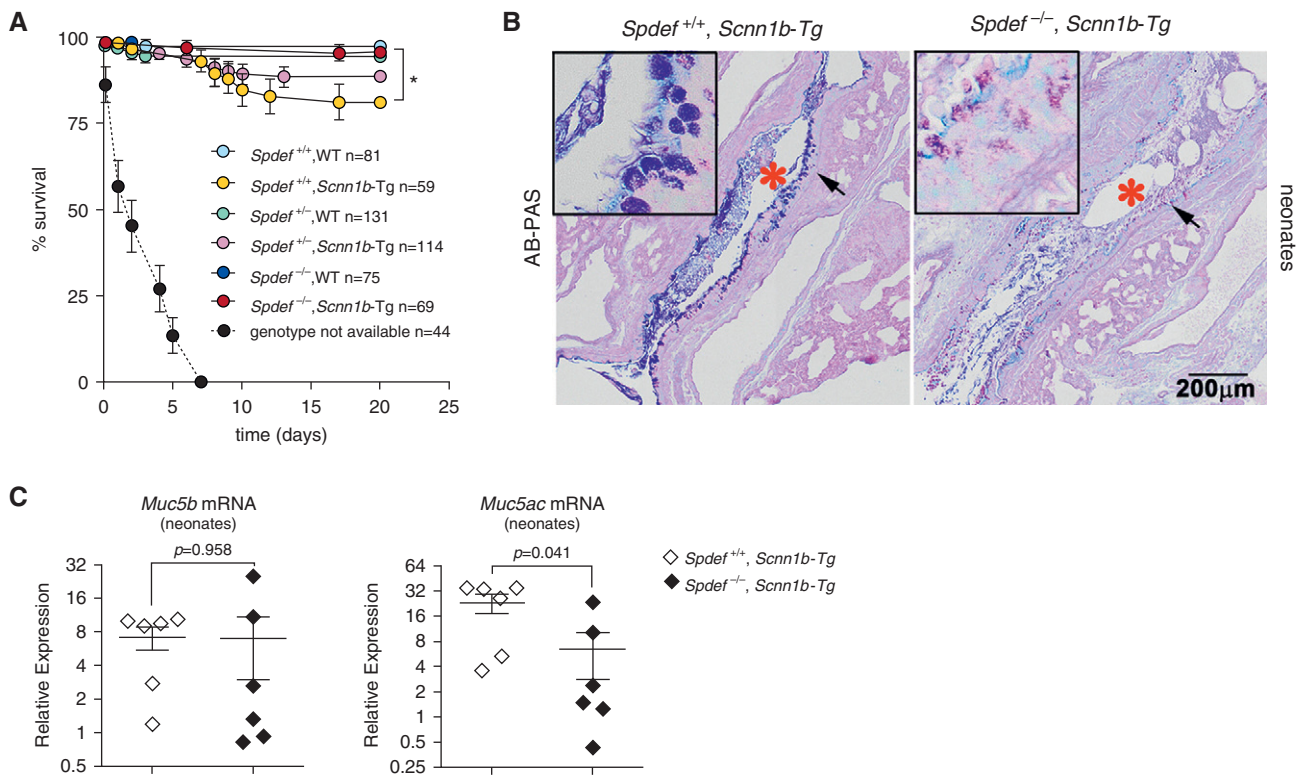
Figure 4. Loss of Spdef improves early survival but fails to decrease airway mucus obstruction in neonatal Scnn1b-transgenic (Scnn1b-Tg) mice. (*A*) Survival curves for the progeny of the $Spdef^{-/-} \times Scnn1b$-Tg cross. *n* = number of mice per genotype. *$P < 0.05$ versus *Spdef*-sufficient ($Spdef^{+/+}$) mice, wild-type (WT) mice by log-rank test. Dashed line indicates survival of mice for which genotypes were not available owing to early death and cannibalization. (*B*) Representative micrographs illustrating AB-PAS staining in neonatal (PND 10) Scnn1b-Tg mice that were either $Spdef^{+/+}$; Scnn1b-Tg or Spdef deficient ($Spdef^{-/-}$; Scnn1b-Tg). Scale bar: 200 μm. *Airway lumen obstructed by mucus plugs. Insets show high-magnification view of areas highlighted by the arrows in the low-magnification panels. Micrographs are representative of at least three mice for each genotype and are montages acquired with a slide scanner, as described in the METHODS section of the text. (*C*) Quantitative RT-PCR results for *Muc5b* and *Muc5ac* transcripts in neonatal (PND 10) Scnn1b-Tg mice that were either $Spdef^{+/+}$; Scnn1b-Tg (open diamond) or $Spdef^{-/-}$; Scnn1b-Tg (solid diamond) (*n* = 5–6/genotype).

from $Spdef^{-/-}$ mice versus their littermates (Figures E3B and E3C). To assess CBF, mTECs were isolated from WT and $Spdef^{-/-}$ mice and cultured under air–liquid interface conditions until fully differentiated. No significant difference in CBF was detected between WT and $Spdef^{-/-}$ mTEC (Figure E3D), suggesting that loss of *Spdef* did not overtly alter CBF.

Loss of Spdef Improved Survival but Did Not Prevent Mucus Obstruction in a Mouse Model of Airway Surface Dehydration

To explore the role of Spdef in Muc5b-dominated mucoobstructive lung disease, we bred $Spdef^{-/-}$ mice to Scnn1b-Tg mice and evaluated the phenotype of the progeny. *Spdef*-deficient Scnn1b-Tg mice

were born at the expected Mendelian proportion, and their survival (~100%) was significantly higher than that of *Spdef*-sufficient Scnn1b-Tg mice (~80%) (Figure 4A).

Both *Spdef*-deficient and *Spdef*-sufficient Scnn1b-Tg mice exhibited airway mucus plugging as early as PND 7 (Figure 4B). Qualitatively, airway mucus

Figure 3. (Continued). (*n* = 5–6/genotype). (*C*) Representative micrographs illustrating AB-PAS (upper panel), Muc5b (middle panel), and Muc5ac (lower panel) staining in the proximal main stem bronchus (left lung) of naive $Spdef^{+/+}$ and $Spdef^{-/-}$ mice at PND 42. Insets show high-magnification views of areas highlighted by the arrows in the low-magnification panels. Micrographs are montages acquired with a slide scanner as described in the METHODS section of the main text. Scale bars: 100 μm. (*D–F*) Morphometric quantification of (*D*) AB-PAS$^+$, (*E*) Muc5b$^+$, and (*F*) Muc5ac$^+$ volume densities in proximal, intermediate, and distal sections of the main stem bronchus in naive Spdef$^{+/+}$ (open dots) and $Spdef^{-/-}$ (solid dots) mice at PND 42. Data are presented as mean ± SEM and were analyzed with an unpaired Student's *t* test. (*G*) Densitometric analysis of Muc5b- and Muc5ac-specific signaling in agarose Western blots of BAL from naive $Spdef^{+/+}$ (open dots) and $Spdef^{-/-}$ (solid dots) mice at 4–5 months of age (*n* = 3–4/genotype). Note that Muc5ac was undetectable for both genotypes in adult mice. (*H*) Quantitative RT-PCR results for Muc5b and Muc5ac transcripts in naive $Spdef^{+/+}$ (open dots) and $Spdef^{-/-}$ (solid dots) mice at PND 42 (*n* = 7–9/genotype). (*I*) Tracheal mucociliary clearance measurements in naive $Spdef^{+/+}$ (open bar) and $Spdef^{-/-}$ (solid bar) adult mice (*n* = 9/genotype) at ages PND 43 (*n* = 7) and PND 170 (*n* = 2) for both genotypes. (*J*) Bioelectrical properties of tracheal epithelium isolated from naive $Spdef^{+/+}$ (open bar) and $Spdef^{-/-}$ (solid bar) mice at 4–5 months of age (*n* = 5–7/genotype). *$P < 0.05$, analyzed with 2 tailed, unpaired Student's *t* test.
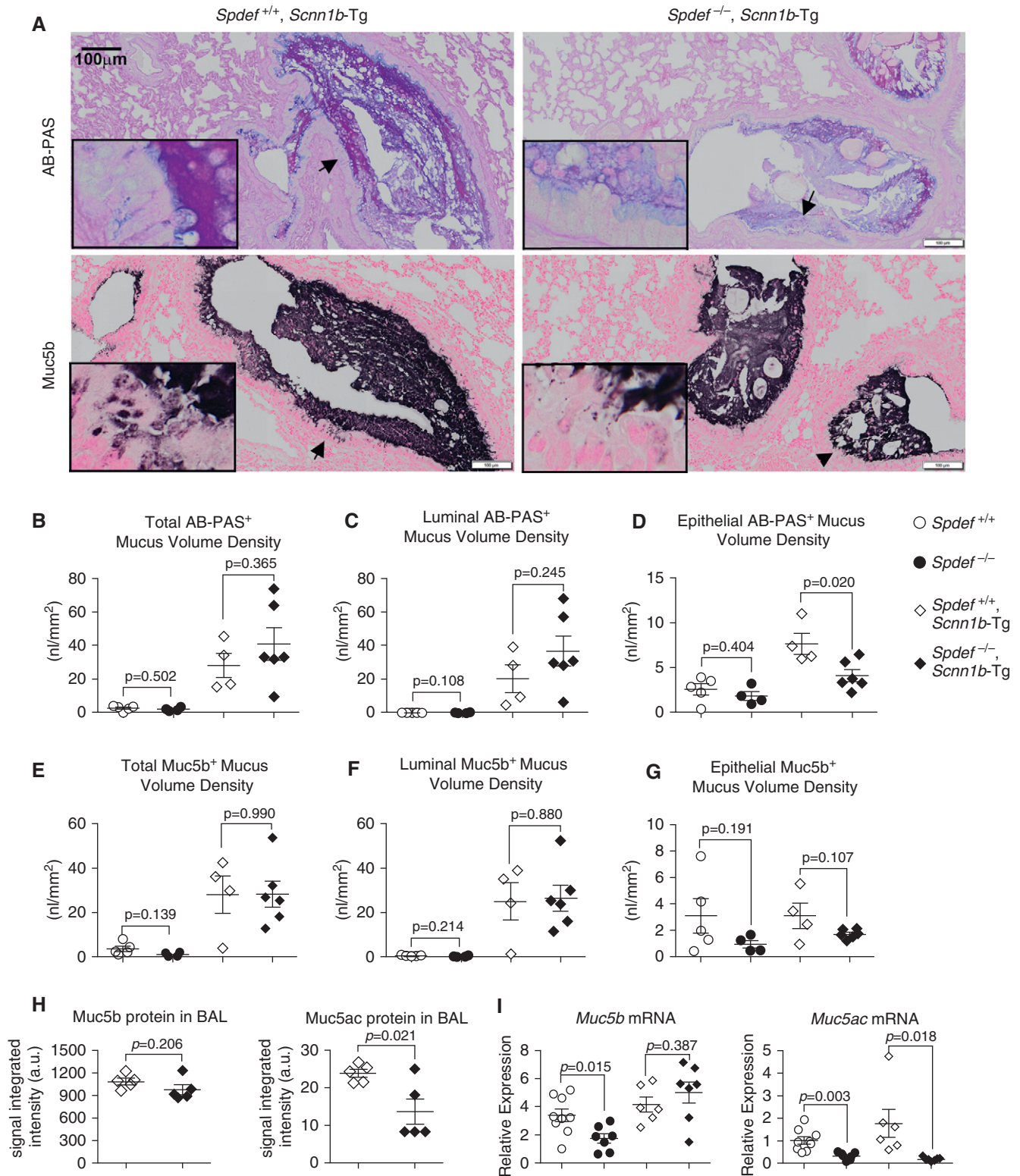
Figure 5. Spdef deficiency does not affect airway mucus obstruction or Muc5b expression in adult *Scnn1b*-Tg mice. (*A*) Representative micrographs illustrating AB-PAS and Muc5b stain in adult (PND 42) *Scnn1b*-Tg mice either Spdef sufficient (*Spdef*$^{+/+}$; *Scnn1b*-Tg) or Spdef deficient (*Spdef*$^{-/-}$; *Scnn1b*-Tg). Scale bars: 100 μm. Insets show high-magnification views of areas highlighted by the arrows in the low-magnification panels. Micrographs are representative of at least three mice for each genotype and are montages acquired with a slide scanner as described in the METHODS section of the text. (*B–G*) Morphometric quantification of AB-PAS$^+$ (*B–D*) and Muc5b$^+$ (*E–G*) cumulative volume densities (i.e., comprising proximal, intermediate, and

plugs in neonatal *Spdef*-deficient *Scnn1b*-Tg mice exhibited a less acidic AB-PAS staining than that of mucus plugs in *Spdef*-sufficient *Scnn1b*-Tg littermates. At the mRNA level, neonatal *Spdef*-deficient *Scnn1b*-Tg mice exhibited a reduction in *Muc5ac* mRNA as compared with *Spdef*-sufficient *Scnn1b*-Tg littermates. However, the dominant secreted mucin in the *Scnn1b*-Tg model (i.e., Muc5b) was unaffected by *Spdef* deficiency (Figure 4C), suggesting that *Muc5b* transcription was supported by a different signaling pathway from very early in the development of mucoobstructive lung disease in this model.

Because *Spdef*-directed therapies are being proposed to alleviate the symptoms of both developing and established mucoobstructive lung disease (43), we characterized the phenotype of adult *Spdef*-sufficient and *Spdef*-deficient *Scnn1b*-Tg mice. AB-PAS staining and immunohistochemistry for Muc5b were performed in sequential cross-sections of the proximal, intermediate, and distal left main stem bronchus (Figures E4A–E4H), and luminal versus epithelial versus total (luminal + epithelial) mucus "burden" was evaluated. Of note, we could not perform parallel Muc5ac immunostaining in *Scnn1b*-Tg mice, because the available antibody for murine Muc5ac recognizes intracellular Muc5ac, but it cannot reliably be used to evaluate Muc5ac in intraluminal mucus plugs, owing to interfering murine IgGs located inside the plug (Figure E5).

Notably, *Spdef* depletion did not alter the airway mucus burden in adult *Scnn1b*-Tg mice, as quantified by morphometric analysis of the luminal versus epithelial compartment after AB-PAS– and Muc5b-specific staining (Figures 5A–5G). Specifically, the bulk of the AB-PAS– and Muc5b-specific signaling was confined to the airway lumen, as previously described (26), and this pattern was conserved in *Spdef*-deficient and *Spdef*-sufficient *Scnn1b*-Tg mice (Figures 5B and 5C vs. 5D and Figures 5E and 5F vs. 5G). In *Spdef*-sufficient *Scnn1b*-Tg mice, epithelial AB-PAS$^+$ V$_S$ was higher than that in WT mice, and *Spdef* deletion was associated with a reduction of this index (Figure 5D). Of note, significant lower epithelial AB-PAS$^+$ V$_S$ was consistently measured in the proximal and intermediate airways of *Spdef*-deficient *Scnn1b*-Tg mice (Figure E4D), whereas Muc5b$^+$ V$_S$ was unaffected (Figures 4G and E4H).

As an alternative index of airway mucus obstruction, BAL levels of secreted Muc5b and Muc5ac were measured. *Spdef*-deficient *Scnn1b*-Tg mice exhibited equivalent levels of Muc5b and reduced levels of Muc5ac in BAL compared with *Spdef*-sufficient *Scnn1b*-Tg mice (Figure 5H). At the transcription level, *Muc5ac* mRNA expression was downregulated in the absence of *Spdef*, whereas *Muc5b* transcription was unchanged (Figure 5I), mirroring the pattern observed in neonatal *Scnn1b*-Tg mice derived from this cross (Figure 4C). Collectively, these studies indicate that *Spdef* did not significantly contribute to *Muc5b* transcriptional regulation, expression, secretion, or intraluminal accumulation in the context of the chronic airway surface dehydration–generated mucoobstructive lung disease characteristic of adult *Scnn1b*-Tg mice. A summary of the mucin expression/secretion and mucus obstruction phenotypes observed for Spdef-deficient and Spdef-sufficient mice at baseline and in the context of *Scnn1b*-Tg mucoobstructive lung disease is provided in Table E1.

To test whether activation of an alternative signaling pathway converging on downstream genes in the *Spdef*–mucin axis could bypass the *Spdef* requirement for Muc5b expression in *Scnn1b*-Tg mice, we tested for nuclear expression of Foxa3 (Forkhead box A3). Foxa3 is a transcription factor with both *Spdef*-dependent and *Spdef*-independent functions whose overexpression has been shown to induce both Muc5b and Muc5ac *in vivo* (20). Immunohistochemical detection indicated no Foxa3 immunostaining in *Spdef*-sufficient or *Spdef*-deficient WT mice (Figures 6A and 6B). Moderate nuclear expression of Foxa3 was detected in the surface airway epithelium of *Spdef*-sufficient *Scnn1b*-Tg mice. This immunostaining was completely lost in the absence of *Spdef* (Figures 6C and 6D). Altogether, these results suggest that in the *Scnn1b*-Tg mouse model, *1*) Foxa3 expression is *Spdef* dependent and *2*) Muc5b expression is both Spdef and Foxa3 independent. Consistent with the results showing complete *Spdef* dependency of Foxa3 expression in adult lung, *Foxa3* mRNA was largely reduced in whole lung from neonatal *Spdef*-deficient mice, regardless of their *Scnn1b*-Tg status (Figure 6E).

Spdef Deletion Increased Airway Neutrophilic Inflammation in Neonatal Scnn1b-Tg Mice

In addition to being a master regulator of mucous cell metaplasia, previous studies have identified a role for Spdef in maintaining immune homeostasis by blunting innate immune responses during inflammatory challenges through cytoplasmic binding to key adaptor molecules (i.e., MyD88) (23). In this study, *Spdef* deficiency alone was not sufficient to cause BAL neutrophilia. However, increased BAL neutrophilia was observed in neonatal *Spdef*-deficient *Scnn1b*-Tg mice as compared with *Spdef*-sufficient *Scnn1b*-Tg littermates (Figure 7A). Although the observation was not significant, neonatal *Spdef*-deficient *Scnn1b*-Tg mice also exhibited a trend toward increased macrophage numbers as compared with *Spdef*-sufficient *Scnn1b*-Tg mice (Figure 7B). No other genotype-dependent differences were detected in the BAL differential cell counts in neonatal or adult mice (Figures 7C and 7D).

Figure 5. (Continued). distal sections of the main stem bronchus) in adult (PND 42) mice from the *Spdef*$^{+/-}$ × *Scnn1b*-Tg cross: *Spdef*$^{+/+}$ (open dots), *Spdef*$^{-/-}$ (solid dots), *Spdef*$^{+/+}$; *Scnn1b*-Tg (open diamonds), or *Spdef*$^{-/-}$; *Scnn1b*-Tg (solid diamonds). For each stain, total (luminal + epithelial; *B* and *E*), luminal-only (*C* and *F*), and epithelial-only (*D* and *G*) volume densities are graphed. Results for individual levels are reported in Figures E4B–E4D and Figures E4F–E4H, respectively. Data are presented as mean ± SEM and were analyzed by unpaired Student's *t* test. (*H*) Densitometric analysis of Muc5b- and Muc5ac-specific signaling in agarose Western blots of BAL from adult (PND 42) *Scnn1b*-Tg mice that were either *Spdef*$^{+/+}$; *Scnn1b*-Tg (open diamonds) or *Spdef*$^{-/-}$; *Scnn1b*-Tg (solid diamonds) (*n* = 5/genotype). (*I*) Quantitative RT-PCR results for *Muc5b* and *Muc5ac* transcripts in adult (PND 42) *Spdef*$^{+/+}$ (open dots), *Spdef*$^{-/-}$ (solid dots), *Spdef*$^{+/+}$; *Scnn1b*-Tg (open diamonds), or *Spdef*$^{-/-}$; *Scnn1b*-Tg (solid diamonds) mice (*n* = 6–9/genotype).
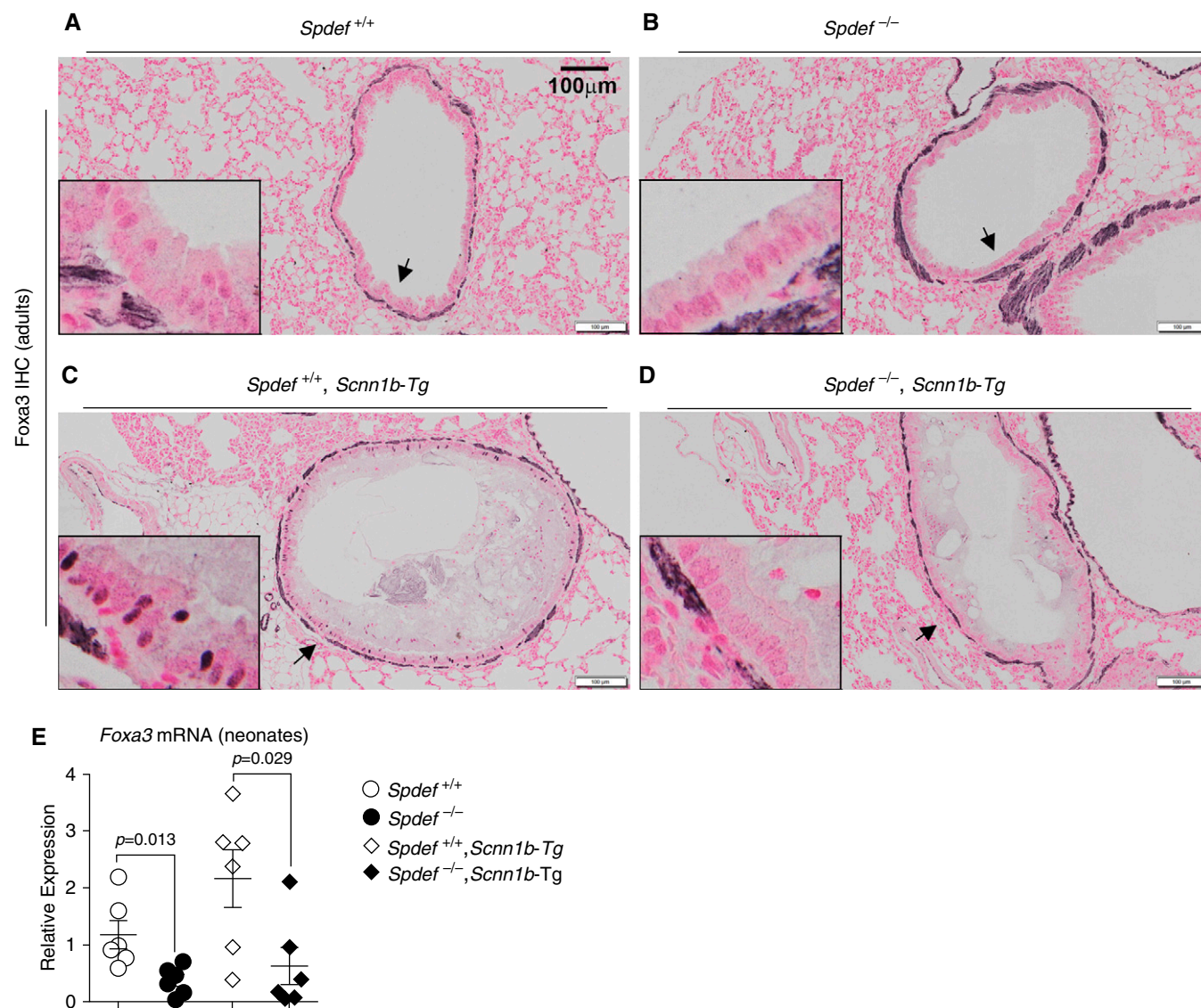
Figure 6. Foxa3 (forkhead box A3) expression in *Scnn1b*-Tg mouse mucus-obstructed airways is Spdef dependent. (*A–D*) Representative micrographs illustrating Foxa3 nuclear staining pattern in adult (PND 42) (*A*) *Spdef*-sufficient (*Spdef*$^{+/+}$; no stain), (*B*) *Spdef*-deficient (*Spdef*$^{-/-}$; no stain), (*C*) *Spdef*-sufficient *Scnn1b*-Tg (*Spdef*$^{+/+}$; *Scnn1b*-Tg; sparse nuclear stain), or (*D*) *Spdef*-deficient *Scnn1b*-Tg (*Spdef*$^{-/-}$; *Scnn1b*-Tg no stain) mice. Scale bars: 100 μm. Insets show high-magnification views of areas highlighted by the arrows in the low-magnification panels. Micrographs are representative of at least three mice for each genotype. Micrographs are montages acquired with a slide scanner as described in the Methods section of the main text. Of note, Foxa3 antibody generated a nonspecific stain in the basement membrane, which was shown to be present in *Foxa3*$^{-/-}$ mice (53). (*E*) Quantitative RT-PCR results for *Foxa3* transcripts in neonatal (PND 10) *Spdef*$^{+/+}$ (open dots), *Spdef*$^{-/-}$ (solid dots), *Spdef*$^{+/+}$; *Scnn1b*-Tg (open diamonds), or *Spdef*$^{-/-}$; *Scnn1b*-Tg (solid diamonds) mice (*n* = 6/genotype).

Discussion

Secretory cells, including mucous secretory cells, are essential in health to maintain proper lubrication and protection of epithelial surfaces, including the intestine, eustachian tubes, and respiratory tract. Although Spdef has been defined as a central transcription factor in mucous cell biology

in a variety of epithelial tissues, molecular complexity likely arises within the Spdef pathway as a result of tissue-specific and health status–specific upstream signals that regulate *Spdef* expression and a multiplicity of downstream targets.

Previous reports indicated that mucin expression in the healthy respiratory tract is developmental stage dependent and region

specific (8, 24, 44, 45). Our results indicate that *Spdef* deficiency also differentially regulates the distribution of mucins in both the upper and lower airways. With reference to the mucin expression in the upper airways (Figures 1A, 1B, and 2A–2E), Spdef appears to regulate expression of Muc5b in the surface epithelium of the nasal septum, anterior nasopharynx, and
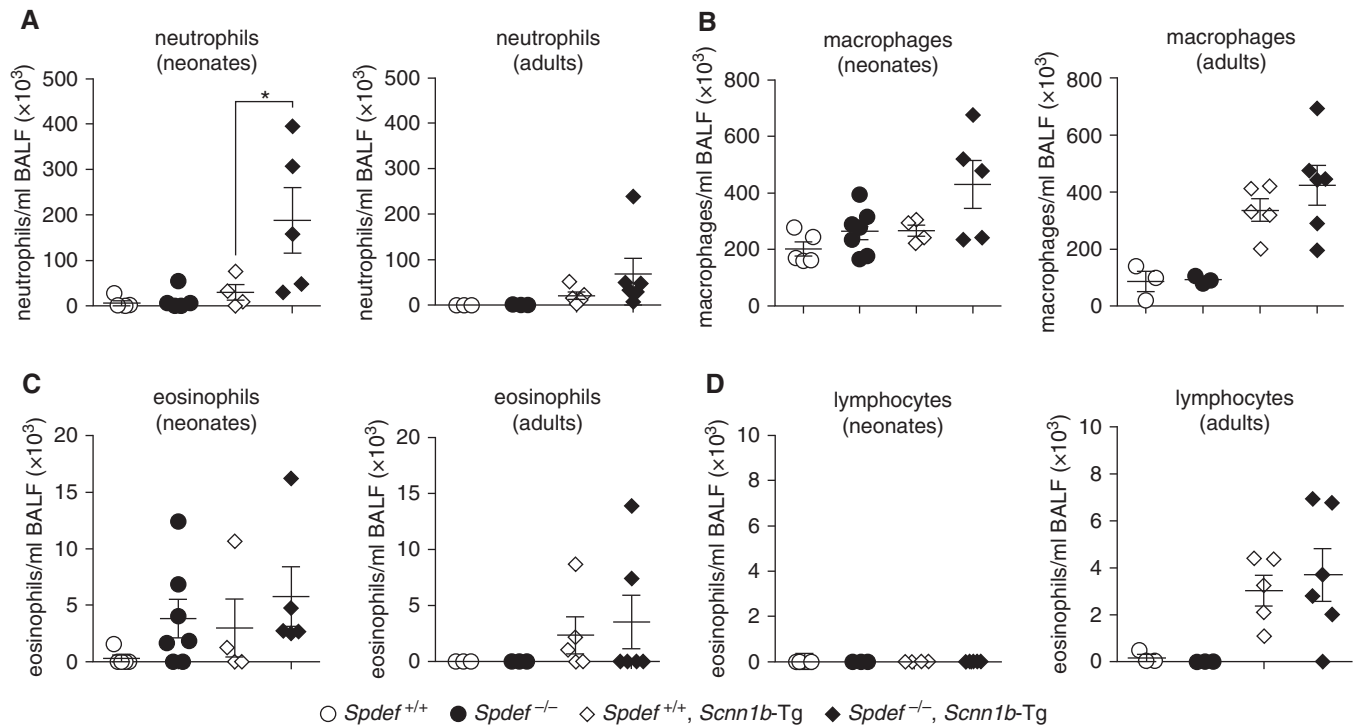
Figure 7. Loss of Spdef increases airway neutrophil infiltration in Scnn1b-Tg mice. (*A–D*) Differential BAL cell counts: (*A*) neutrophils, (*B*) macrophages, (*C*) eosinophils, and (*D*) lymphocytes in neonatal (PND 7–10; left panel) or adult (PND 120–170; right panel) mice from the $Spdef^{+/-} \times Scnn1b$-Tg cross: $Spdef$-sufficient ($Spdef^{+/+}$; open dots), $Spdef$-deficient ($Spdef^{-/-}$; solid dots), $Spdef$-sufficient $Scnn1b$-Tg ($Spdef^{+/+}$; $Scnn1b$-Tg open diamonds), or $Spdef$-deficient $Scnn1b$-Tg ($Spdef^{-/-}$; $Scnn1b$-Tg solid diamonds). *$P < 0.05$ versus $Spdef^{+/+}$; $Scnn1b$-Tg mice by one way ANOVA. BALF = BAL fluid.

trachea, as well as in the mucus-secreting cells of the submucosal glands, but not in the Bowman glands associated with the olfactory epithelium. Similar to its role in the tracheal compartment, Muc5b was the dominant expressed mucin in the murine lower airways (Figure 3).

Spdef deletion resulted in lower basal Muc5b mRNA expression (Figure 3H), intraepithelial content (especially in the proximal airways; Figure 3E), and BAL content in both neonatal and adult naive $Spdef^{-/-}$ mice than in WT littermates (Figures 3B and 3G). A shift toward a less acidic AB-PAS staining pattern was observed in both neonatal (Figure 3A) and adult (Figure 3C, upper panel) $Spdef^{-/-}$ mice, which may reflect $Spdef$-dependent downregulation of key glycosylation enzymes and reduced mucin glycosylation (17, 20).

Intriguingly, $Spdef^{-/-}$ mice partially phenocopied $Muc5b^{-/-}$ mice, as exhibited by decreased Muc5b expression (Figures 1B, 3E, and 3G), distinctive nasopharyngeal hair/mucus plugs (Figure 1C), and a milder but detectable otitis media (Figure 1D), and

defective tracheal MCC (Figure 3I). However, they did not exhibit MCC defects in the anterior nasopharynx (Figure 1E) or abnormalities in the olfactory epithelium Bowman glands (Figures 1A and 1B). The retention of Muc5b expression in Bowman glands points to redundant or alternative control of Muc5b expression in this tissue. It is of interest that both the $Muc5b^{-/-}$ mice and the $Spdef^{-/-}$ mice exhibited nasopharyngeal hair/mucus plugs, but $Spdef^{-/-}$ mice did so in the absence of defective anterior nasopharynx MCC. Clearly, the presence or absence of MCC was not the sole determinant of hair/mucus plug formation in the posterior nasopharynx, because mice with amotile cilia, and thus no MCC, do not form hair/mucus plugs (B. Grubb, unpublished results). We speculate that the most important contributor to hair/mucus plug formation is the composition of surface mucus, which acts as a lubricant to facilitate transport of hair/debris through the distal portion of the nasopharynx, possibly by muscular propulsion. In this context, $Spdef$ depletion may have altered mucus

composition (in terms of both mucins and ancillary proteins [46]), overall hydration, or glycosylation, which affected its lubricating function.

The observed defect in tracheal MCC led to the discovery of another unexpected phenotype in naive $Spdef^{-/-}$ mice—that is, the ion transport abnormalities indicative of increased Na^+ absorption (amiloride-sensitive I_{sc}) and Cl^- secretion (forskolin-stimulated I_{sc})—in tracheas studied *ex vivo* (Figure 3J). Previous studies have suggested that ciliated cells are the main source of the ion transport properties of the airways (47). Thus, the simplest explanation for increased Na^+ absorption and Cl^- secretion in the $Spdef^{-/-}$ mice is an increase in the density of ciliated cells per unit of surface area. However, measurement of the density of acetylated α-tubulin$^+$ ciliated cells in the portion of the trachea used to measure bioelectrical properties failed to reveal significant differences in cell distribution between $Spdef$-deficient and $Spdef$-sufficient mice (Figures E3B and E3C). It is also possible that Spdef-dependent transcriptional

regulation of ENaC contributed to this phenotype. However, the modest upregulation of α-ENaC in the absence of *Spdef* appears unlikely to raise Na^+ transport rates. Regardless, owing to the balanced increase in Na^+ absorption and Cl^- secretion, the overall airway surface hydration status likely was not significantly altered in $Spdef^{-/-}$ mice. Therefore, it is likely that reduced Muc5b expression in the tracheal surface epithelium (Figure 2D) was the main cause of the reduction in MCC in *Spdef*-deficient mice.

Many human mucoobstructive lung diseases, such as chronic bronchitis, cystic fibrosis, and primary ciliary dyskinesia, appear to be characterized by intrapulmonary accumulations of hyperconcentrated mucins, often dominated by MUC5B (33–35).These diseases appear to reflect in part abnormalities in both Na^+ absorption and Cl^- secretion that produce ASL depletion (i.e., "dehydration"), with concomitant mucus-mucin hyperconcentration (48, 49). To investigate the role of Spdef in a mouse model dominated by ASL dehydration and Muc5b accumulation (26), *Spdef*-deficient mice were crossed with *Scnn1b*-Tg mice. These studies indicated that the dependence of Muc5b expression on *Spdef* differed in health versus disease. In contrast to naive $Spedf^{-/-}$ mice (Figures 3B and 3H), *Spdef* deficiency did not affect *Muc5b* mRNA expression in either neonatal or adult *Scnn1b*-Tg mice (Figures 4C and 5I), nor did it affect Muc5b protein as measured by intraluminal or intraepithelial content (Figures 5A and 5E–5G) and BAL levels (Figure 5H) in adult mice. Thus, we hypothesize that the complex inflammatory milieu associated with *Scnn1b*-Tg mucoobstructive lung disease (50) bypassed Spdef (and Foxa3) in

regulating Muc5b transcription. Thus, the failure of *Spdef* deficiency to abolish airway mucus obstruction in *Scnn1b*-Tg mice likely reflects sustained expression/secretion of Muc5b, perhaps in part due to hypoxia-mediated mechanisms (51, 52), coupled to failed clearance due to mucus dehydration.

Unlike Muc5b, Muc5ac protein and mRNA levels were reduced in *Spdef*-deficient *Scnn1b*-Tg mice (Figures 4C, 5H, and 5I), which paralleled the findings in naive *Spdef*-deficient mice (Figures 3B, 3G, and 3H). Our previous data for Muc5ac-deficient *Scnn1b*-Tg mice suggested that Muc5ac has a temporally confined contribution to the obstructive lung pathology of *Scnn1b*-Tg mice because it supports the formation of tracheal mucus plugging associated with neonatal mortality in *Scnn1b*-Tg mice (26). Both $Muc5ac^{-/-}$ mice and neonatal *Spdef*-deficient *Scnn1b*-Tg mice exhibit a neonatal survival advantage as compared with their *Spdef*-sufficient *Scnn1b*-Tg littermates (Figure 4A). These data suggest that *Spdef* regulation of Muc5ac contributed to the poor survival of neonatal *Spdef*-sufficient *Scnn1b*-Tg mice.

The *Spdef* deletion–dependent downregulation of Muc5ac expression, however, had little effect on the adult phenotype of *Scnn1b*-Tg mice, as assessed by immunohistochemistry and morphometry. Indirect evidence of Spdef-dependent Muc5ac regulation in adult *Scnn1b*-Tg mice emerged from morphometric studies that showed a consistent decrease in proximal and intermediate epithelial AB-PAS$^+$ V_S in *Spdef*-deficient *Scnn1b*-Tg mice as compared with *Spdef*-sufficient *Scnn1b*-Tg mice. Because this pattern was not paralleled by a similar change in Muc5b$^+$

V_S, the decreased AB-PAS staining could reflect loss of Muc5ac and/or loss of acidic post-translational modification.

Interestingly, despite the survival advantage, *Spdef* deletion resulted in increased airway neutrophilia in neonatal *Scnn1b*-Tg mice (Figure 7A). This result suggests that loss of the Spdef-dependent innate immune suppression of inflammation (23) produced a potentially detrimental hyperinflammatory response.

In summary, our data show that Spdef-dependent regulation of Muc5ac and Muc5b expression in the airways was tissue specific and disease dependent. We hypothesize that the consequences of *Spdef* depletion in airway mucous cell biology depend both on regulation of mucin transcription and on other related processes, such as mucin glycosylation. Moreover, our data suggest that *Spdef* may not be an effective therapeutic target for conditions characterized by Muc5b-dominated airway mucus hypersecretion and obstruction. ■

References

1. Rubin BK. Secretion properties, clearance, and therapy in airway disease. *Transl Respir Med* 2014;2:6.
2. Button B, Anderson WH, Boucher RC. Mucus hyperconcentration as a unifying aspect of the chronic bronchitic phenotype. *Ann Am Thorac Soc* 2016;13(Suppl 2):S156–S162.
3. Seibold MA, Wise AL, Speer MC, Steele MP, Brown KK, Loyd JE, et al. A common MUC5B promoter polymorphism and pulmonary fibrosis. *N Engl J Med* 2011;364:1503–1512.
4. Thornton DJ, Rousseau K, McGuckin MA. Structure and function of the polymeric mucins in airways mucus. *Annu Rev Physiol* 2008;70:459–486.
5. Kreda SM, Davis CW, Rose MC. CFTR, mucins, and mucus obstruction in cystic fibrosis. *Cold Spring Harb Perspect Med* 2012;2:a009589.
6. Widdicombe JH, Wine JJ. Airway gland structure and function. *Physiol Rev* 2015;95:1241–1319.
7. Roy MG, Livraghi-Butrico A, Fletcher AA, McElwee MM, Evans SE, Boerner RM, et al. Muc5b is required for airway defence. *Nature* 2014; 505:412–416.
8. Roy MG, Rahmani M, Hernandez JR, Alexander SN, Ehre C, Ho SB, et al. Mucin production during prenatal and postnatal murine lung development. *Am J Respir Cell Mol Biol* 2011;44: 755–760.
9. Zhu Y, Abdullah LH, Doyle SP, Nguyen K, Ribeiro CM, Vasquez PA, et al. Baseline goblet cell mucin secretion in the airways exceeds stimulated secretion over extended time periods, and is sensitive to shear stress and intracellular mucin stores. *PLoS One* 2015;10: e0127267.

10. Chen Y, Zhao YH, Di YP, Wu R. Characterization of human mucin 5b gene expression in airway epithelium and the genomic clone of the amino-terminal and 5′-flanking region. *Am J Respir Cell Mol Biol* 2001;25:542–553.

11. Groneberg DA, Eynott PR, Oates T, Lim S, Wu R, Carlstedt I, et al. Expression of MUC5AC and MUC5B mucins in normal and cystic fibrosis lung. *Respir Med* 2002;96:81–86.

12. Curran DR, Cohn L. Advances in mucous cell metaplasia: a plug for mucus as a therapeutic focus in chronic airway disease. *Am J Respir Cell Mol Biol* 2010;42:268–275.

13. McCauley HA, Guasch G. Three cheers for the goblet cell: maintaining homeostasis in mucosal epithelia. *Trends Mol Med* 2015;21:492–503.

14. Oettgen P, Finger E, Sun Z, Akbarali Y, Thamrongsak U, Boltax J, et al. PDEF, a novel prostate epithelium-specific Ets transcription factor, interacts with the androgen receptor and activates prostate-specific antigen gene expression. *J Biol Chem* 2000;275:1216–1225.

15. Aronson BE, Stapleton KA, Vissers LA, Stokhuijzen E, Bruijnzeel H, Krasinski SD. *Spdef* deletion rescues the crypt cell proliferation defect in conditional *Gata6* null mouse small intestine. *BMC Mol Biol* 2014;15:3.

16. Marko CK, Menon BB, Chen G, Whitsett JA, Clevers H, Gipson IK. *Spdef* null mice lack conjunctival goblet cells and provide a model of dry eye. *Am J Pathol* 2013;183:35–48.

17. Chen G, Korfhagen TR, Xu Y, Kitzmiller J, Wert SE, Maeda Y, et al. SPDEF is required for mouse pulmonary goblet cell differentiation and regulates a network of genes associated with mucus production. *J Clin Invest* 2009;119:2914–2924.

18. Noah TK, Kazanjian A, Whitsett J, Shroyer NF. SAM pointed domain ETS factor (SPDEF) regulates terminal differentiation and maturation of intestinal goblet cells. *Exp Cell Res* 2010;316:452–465.

19. Gregorieff A, Stange DE, Kujala P, Begthel H, van den Born M, Korving J, et al. The Ets-domain transcription factor Spdef promotes maturation of goblet and Paneth cells in the intestinal epithelium. *Gastroenterology* 2009;137:1333–1345.e1–1345.e3.

20. Rajavelu P, Chen G, Xu Y, Kitzmiller JA, Korfhagen TR, Whitsett JA. Airway epithelial SPDEF integrates goblet cell differentiation and pulmonary Th2 inflammation. *J Clin Invest* 2015;125:2021–2031.

21. Vock C, Yildirim AO, Wagner C, Schlick S, Lunding LP, Lee CG, et al. Distal airways are protected from goblet cell metaplasia by diminished expression of IL-13 signalling components. *Clin Exp Allergy* 2015;45:1447–1458.

22. Park KS, Korfhagen TR, Bruno MD, Kitzmiller JA, Wan H, Wert SE, et al. SPDEF regulates goblet cell hyperplasia in the airway epithelium. *J Clin Invest* 2007;117:978–988.

23. Korfhagen TR, Kitzmiller J, Chen G, Sridharan A, Haitchi HM, Hegde RS, et al. SAM-pointed domain ETS factor mediates epithelial cell-intrinsic innate immune signaling during airway mucous metaplasia. *Proc Natl Acad Sci USA* 2012;109:16630–16635.

24. Livraghi A, Grubb BR, Hudson EJ, Wilkinson KJ, Sheehan JK, Mall MA, et al. Airway and lung pathology due to mucosal surface dehydration in β-epithelial Na$^+$ channel-overexpressing mice: role of TNF-α and IL-4Rα signaling, influence of neonatal development, and limited efficacy of glucocorticoid treatment. *J Immunol* 2009;182:4357–4367.

25. Livraghi-Butrico A, Grubb BR, Kelly EJ, Wilkinson KJ, Yang H, Geiser M, et al. Genetically determined heterogeneity of lung disease in a mouse model of airway mucus obstruction. *Physiol Genomics* 2012;44:470–484.

26. Livraghi-Butrico A, Grubb BR, Wilkinson KJ, Volmer AS, Burns KA, Evans CM, et al. Contribution of mucus concentration and secreted mucins Muc5ac and Muc5b to the pathogenesis of muco-obstructive lung disease. *Mucosal Immunol* 2017;10:395–407.

27. Livraghi-Butrico A, Kelly EJ, Klem ER, Dang H, Wolfgang MC, Boucher RC, et al. Mucus clearance, MyD88-dependent and MyD88-independent immunity modulate lung susceptibility to spontaneous bacterial infection and inflammation. *Mucosal Immunol* 2012;5:397–408.

28. Livraghi-Butrico A, Kelly EJ, Wilkinson KJ, Rogers TD, Gilmore RC, Harkema JR, et al. Loss of *Cftr* function exacerbates the phenotype of Na$^+$ hyperabsorption in murine airways. *Am J Physiol Lung Cell Mol Physiol* 2013;304:L469–L480.

29. Mall M, Grubb BR, Harkema JR, O'Neal WK, Boucher RC. Increased airway epithelial Na$^+$ absorption produces cystic fibrosis-like lung disease in mice. *Nat Med* 2004;10:487–493.

30. Mall MA, Harkema JR, Trojanek JB, Treis D, Livraghi A, Schubert S, et al. Development of chronic bronchitis and emphysema in β-epithelial Na$^+$ channel-overexpressing mice. *Am J Respir Crit Care Med* 2008;177:730–742.

31. Esther CR Jr, Hill DB, Button B, Shi S, Jania C, Duncan EA, et al. The sialic acid-to-urea ratio as a measure of airway surface hydration. *Am J Physiol Lung Cell Mol Physiol* 2017;312:L398–L404.

32. Anderson WH, Coakley RD, Button B, Henderson AG, Zeman KL, Alexis NE, et al. The relationship of mucus concentration (hydration) to mucus osmotic pressure and transport in chronic bronchitis. *Am J Respir Crit Care Med* 2015;192:182–190.

33. Henderson AG, Ehre C, Button B, Abdullah LH, Cai LH, Leigh MW, et al. Cystic fibrosis airway secretions exhibit mucin hyperconcentration and increased osmotic pressure. *J Clin Invest* 2014;124:3047–3060.

34. Kirkham S, Kolsum U, Rousseau K, Singh D, Vestbo J, Thornton DJ. MUC5B is the major mucin in the gel phase of sputum in chronic obstructive pulmonary disease. *Am J Respir Crit Care Med* 2008;178:1033–1039.

35. Kesimer M, Ford AA, Ceppe A, Radicioni G, Cao R, Davis CW, et al. Airway mucin concentration as a marker of chronic bronchitis. *N Engl J Med* 2017;377:911–922.

36. Mery S, Gross EA, Joyner DR, Godo M, Morgan KT. Nasal diagrams: a tool for recording the distribution of nasal lesions in rats and mice. *Toxicol Pathol* 1994;22:353–372.

37. Donoghue LJ, Livraghi-Butrico A, McFadden KM, Thomas JM, Chen G, Grubb BR, et al. Identification of *trans* protein QTL for secreted airway mucins in mice and a causal role for *Bpifb1*. *Genetics* 2017;207:801–812.

38. Grubb BR, Livraghi-Butrico A, Rogers TD, Yin W, Button B, Ostrowski LE. Reduced mucociliary clearance in old mice is associated with a decrease in Muc5b mucin. *Am J Physiol Lung Cell Mol Physiol* 2016;310:L860–L867.

39. Grubb BR, Paradiso AM, Boucher RC. Anomalies in ion transport in CF mouse tracheal epithelium. *Am J Physiol* 1994;267:C293–C300.

40. You Y, Brody SL. Culture and differentiation of mouse tracheal epithelial cells. *Methods Mol Biol* 2013;945:123–143.

41. Ostrowski LE, Yin W, Rogers TD, Busalacchi KB, Chua M, O'Neal WK, et al. Conditional deletion of *Dnaic1* in a murine model of primary ciliary dyskinesia causes chronic rhinosinusitis. *Am J Respir Cell Mol Biol* 2010;43:55–63.

42. Livraghi-Butrico A, Wilkinson KJ, Volmer AS, Gilmore RC, Rogers TD, Caldwell RA, et al. Lung disease phenotypes caused by overexpression of combinations of α-, β-, and γ-subunits of the epithelial sodium channel in mouse airways. *Am J Physiol Lung Cell Mol Physiol* 2017;314:L318–L331.

43. Song J, Cano-Rodriquez D, Winkle M, Gjaltema RA, Goubert D, Jurkowski TP, et al. Targeted epigenetic editing of SPEDF reduces mucus production in lung epithelial cells. *Am J Physiol Lung Cell Mol Physiol* 2017;312:L334–L347.

44. Buisine MP, Devisme L, Copin MC, Durand-Reville M, Gosselin B, Aubert JP, et al. Developmental mucin gene expression in the human respiratory tract. *Am J Respir Cell Mol Biol* 1999;20:209–218.

45. Reid CJ, Gould S, Harris A. Developmental expression of mucin genes in the human respiratory tract. *Am J Respir Cell Mol Biol* 1997;17:592–598.

46. Radicioni G, Cao R, Carpenter J, Ford AA, Wang TT, Li Y, et al. The innate immune properties of airway mucosal surfaces are regulated by dynamic interactions between mucins and interacting proteins: the mucin interactome. *Mucosal Immunol* 2016;9:1442–1454.

47. Enuka Y, Hanukoglu I, Edelheit O, Vaknine H, Hanukoglu A. Epithelial sodium channels (ENaC) are uniformly distributed on motile cilia in the oviduct and the respiratory airways. *Histochem Cell Biol* 2012;137:339–353.

48. Hobbs CA, Da Tan C, Tarran R. Does epithelial sodium channel hyperactivity contribute to cystic fibrosis lung disease? *J Physiol* 2013;591:4377–4387.

49. Tarran R, Sabater JR, Clarke TC, Tan CD, Davies CM, Liu J, *et al*. Nonantibiotic macrolides prevent human neutrophil elastase-induced mucus stasis and airway surface liquid volume depletion. *Am J Physiol Lung Cell Mol Physiol* 2013;304:L746–L756.

50. Saini Y, Dang H, Livraghi-Butrico A, Kelly EJ, Jones LC, O'Neal WK, *et al*. Gene expression in whole lung and pulmonary macrophages reflects the dynamic pathology associated with airway surface dehydration. *BMC Genomics* 2014;15:726.

51. Montgomery ST, Mall MA, Kicic A, Stick SM; AREST CF. Hypoxia and sterile inflammation in cystic fibrosis airways: mechanisms and potential therapies. *Eur Respir J* 2017;49:1600903.

52. Fritzsching B, Zhou-Suckow Z, Trojanek JB, Schubert SC, Schatterny J, Hirtz S, *et al*. Hypoxic epithelial necrosis triggers neutrophilic inflammation via IL-1 receptor signaling in cystic fibrosis lung disease. *Am J Respir Crit Care Med* 2015;191:902–913.

53. Chen G, Korfhagen TR, Karp CL, Impey S, Xu Y, Randell SH, *et al*. Foxa3 induces goblet cell metaplasia and inhibits innate antiviral immunity. *Am J Respir Crit Care Med* 2014;189:301–313.